Coastal Engineering 43 (2001) 75–92

Coastal Engineering
An International Journal for Coastal, Harbour and Offshore Engineers

www.elsevier.com/locate/coastaleng

Bottom friction in random waves plus current flow

Dag Myrhaug [a,*], Lars Erik Holmedal [a], Richard R. Simons [b], Ruairi D. MacIver [b]

[a] Department of Marine Hydrodynamics, Norwegian University of Science and Technology, N-7491 Trondheim, Norway
[b] Department of Civil and Environmental Engineering, University College London, Gower Street, London WC1E 6BT, UK

Received 29 March 2000; received in revised form 6 February 2001; accepted 23 February 2001

Abstract

Bottom friction in random waves plus current flow is presented. The model is an extension of the Myrhaug [Coastal Eng. 24 (1995) 259] approach for random waves alone. The effect of random waves on the bottom friction is studied by assuming the wave motion to be a stationary Gaussian narrow-band random process, and by using friction coefficient formulas for sinusoidal waves. The data used for comparison are obtained from statistical analysis of direct measurements of bottom shear stresses made in the UK Coastal Research Facility under combined random waves and orthogonal as well as near-orthogonal currents. © 2001 Elsevier Science B.V. All rights reserved.

Keywords: Random waves; Current; Bottom friction; Statistical analysis

1. Introduction

The wave boundary layer affects many phenomena in coastal and offshore engineering as well as in oceanography, e.g., sediment transport, pipeline stability, etc. The wave boundary layer has been studied by itself and also in combination with the current boundary layer as the flow from waves interacting with currents represents the most common flow condition on the seabed for shallow and intermediate water depths, i.e., in coastal zones and on continental shelves.

Reviews of the combined wave and current boundary layer on the seabed are given in Nielsen (1992) and Soulsby et al. (1993). There have been many laboratory experiments specifically on the wave boundary layer, among which Jensen et al. (1989) represents the most recent and detailed experimental investigation. Results from measurements in the ocean have been reported by Lambrakos (1982), Myrhaug et al. (1992) as well as Trowbridge and Agrawal (1995). Theoretical modelling of the wave boundary layer ranges from simple eddy viscosity models to refined turbulence modelling techniques. Reviews of wave boundary layers are given in Nielsen (1992) and Sleath (1995).

Studies on the effect of the randomness of the wave motion on the bottom friction have recently been made. Among these are Zhao and Anastasiou (1993), Ockenden and Soulsby (1994), Simons et al. (1994, 1996), Madsen (1994), Myrhaug (1995) (hereafter denoted as M95), Myrhaug et al. (1998) and Holmedal et al. (2000).

* Corresponding author. Tel.: +47-7359-5527; fax: +47-7359-5528.
E-mail address: dagmyr@marin.ntnu.no (D. Myrhaug).

0378-3839/01/$ - see front matter
PII: S0378-3839(01)00007-2

This paper focuses on the bed shear maxima under random waves plus a relatively weak current using a parametric representation based on experimental data. The approach does not give any information about the boundary layer flow dynamics itself, but the bed shear stress maximum can be estimated to a degree of accuracy suitable for many practical purposes. The maximum bed shear stress is the quantity of primary interest when, e.g., assessing sediment mobility at the seabed.

More specifically, the paper presents the probability distribution function of bed shear stress maxima for random waves plus current, and is valid when the wave bed shear stress is much larger than the current bed shear stress. This is the case when the wave friction factor is much larger than the current friction factor and the wave to current velocity ratio exceeds one over wide ranges of the bed orbital displacement amplitude to roughness ratio as well as the bed roughness to water depth ratio. The model is an extension of M95 for waves alone describing the waves as a stationary Gaussian narrow-band random process, and applies friction coefficient formulas for sinusoidal waves, which are used to derive the distribution function of bed shear stress maxima analytically. Direct laboratory measurements of bottom shear stresses under combined random waves and orthogonal as well as near-orthogonal currents from Simons et al. (1996) and new experiments are used for comparison. Statistical analysis of the data has been performed in order to make a proper comparison with the theoretical approach. The probability distributions of the bed shear stress maxima for individual random waves together with some characteristic statistical values of the bed shear stress maxima are presented. Comparisons are also made with friction coefficients based on characteristic statistical values versus characteristic statistical orbital displacement amplitude to roughness ratio and data, as well as formulas for regular waves.

2. Shear stress distribution under random waves plus current

2.1. Theoretical background for random waves alone

The theoretical background for random waves alone is given in M95 and is summarized here.

The wave friction factor f_w is related to the maximum bottom shear stress induced by individual random waves, τ_m, as

$$\frac{\tau_m}{\rho} = \frac{1}{2} f_w U^2, \tag{1}$$

where ρ is the density of the fluid, U is the bed orbital velocity amplitude, and f_w is taken as

$$f_w = c\left(\frac{A}{z_0}\right)^{-d}. \tag{2}$$

Here c and d are constants, A is the bed orbital displacement amplitude, and z_0 is the seabed roughness parameter. M95 used

$$c = 1.39, \qquad d = 0.52, \tag{3}$$

proposed by Soulsby (1997). This equation is valid for sinusoidal waves and rough turbulent flow, obtained as best fit to data in the range $10 \lesssim A/z_0 \lesssim 10^5$. The data covering the lower A/z_0 values from 10 to 100 are those by Bagnold (1946), Kamphuis (1975) and Simons et al. (1988) (see Soulsby et al., 1993, Fig. 9; Soulsby, 1997).

The dimensionless maximum bottom shear stress for individual random waves is defined as

$$t = \frac{\tau_m}{\frac{1}{2}\rho U_{rms}^2}, \tag{4}$$

where U_{rms} is the rms (root-mean-square) value of U. By assuming the free surface elevation to be a stationary Gaussian narrow-band random process, it follows that the (instantaneous) time-dependent bed orbital displacement a and velocity u are stationary Gaussian narrow-band processes as well. Consequently, the amplitudes A and U are both Rayleigh distributed, i.e.,

$$P(\hat{x}) = 1 - \exp(-\hat{x}^2); \quad \hat{x} = x/x_{rms} \geq 0, \tag{5}$$

where x represents A or U, and x_{rms} represents A_{rms} or U_{rms}. For a narrow-band process, harmonic waves with slowly varying amplitude and phase in time are considered. Then, to the first order, the amplitudes U and A are related by $U = \omega A$ (M95). Furthermore, ω is taken as the mean zero-crossing wave frequency $\omega_z = U_{rms}/A_{rms}$. One should note that this relationship for ω_z is valid for a stationary Gaussian stochastic process. By transformation of random variables, M95 found that t was Weibull distributed with the probability distribution function

$$P(t) = 1 - \exp\left[-\left(\frac{t}{\alpha}\right)^{\beta}\right]; \qquad t \geq 0, \tag{6}$$

with the Weibull parameters

$$\alpha = c\left(\frac{A_{rms}}{z_0}\right)^{-d}, \tag{7}$$

$$\beta = \frac{2}{2-d}. \tag{8}$$

Some other aspects as well as characteristic statistical values are given in the Appendix A.

One should note that the assumptions made here give the basis for the theoretical approach when a current is included. In the forthcoming, this approach will be compared with data.

2.2. Experimental and physical background for extension of M95

Data reported in the present paper are from two series of laboratory measurements of bottom shear stresses under random waves plus current for fully rough turbulent flow conditions. The first set has been reported previously by Simons et al. (1996), while the second set comes from new tests performed as part of the present research programme. Hereafter, these data sets will be referred to as LUCIO and MAST3, respectively, and will now be presented and discussed.

Both sets of experiments were performed in the UK Coastal Research Facility. This is a wave basin measuring 56 × 30 m in plan, equipped with a directional random wave generator, a gently sloping beach for wave absorption, and a current recirculation system allowing fine control over the strength and distribution of longshore current. Still water depth was maintained at 0.5 m over the horizontal bed region in which the shear stress measurements were made. For all the tests, the bed roughness was nominal 1.0 cm diameter granite chippings, fixed to the bed of the basin and to the surface of the shear plate device, with an observed Nikuradse sand roughness $k_N = 1.87$ cm and $z_0 = k_N/30 = 0.0623$ cm. Velocities were recorded using three-component acoustic Doppler velocimeters (ADV) deployed on an instrument carriage which could be located at any point within the test area.

Bottom shear stresses were measured directly using the shear plate device described by Grass et al. (1995). The active element of this instrument is a thin metal disc supported with its upper face parallel with the surrounding bed of the basin. The actual shear stress used in the present analysis has been obtained by correcting the total force exerted on the active element for the pressure gradient effects experienced in unsteady flow. With the active element covered with roughness elements, the pressure correction is equated to the fluid inertia, calculated using the volume of plate plus granite chippings and the fluid acceleration recorded above the centre of

Table 1
Main flow variables and results for: Simons et al. (1996) LUCIO data, where $271 \leq Re \leq 1580$; MAST3 data, where $230 \leq Re \leq 1142$
For both data sets, $z_0 = 0.0623$ cm.

Data set	Record	N	T_z (s)	θ_{wc} (°)	$\overline{U}$ (cm/s)	U_{rms} (cm/s)	A_{rms}/z_0	c	d	β
LUCIO	BEDFR1	202	1.91	–	0	19.70	105.5	19.3	1.02	2.04
	BEDFR2	176	1.83	90	12.5	20.62	106.2	19.6	1.04	2.08
	BEDFR3	221	2.03	–	0	17.66	100.4	18.0	1.00	2.00
	BEDFR4	196	1.92	90	12.6	17.78	95.7	12.1	0.91	1.84
MAST3	t1030W	783	1.22	–	0.6	8.28	25.87	11.39	0.91	1.83
	t2030OC	695	1.22	112.6	13.5	8.20	25.62	13.36	0.95	1.90
	t3030FC	617	1.21	76.3	15.2	8.47	26.18	14.63	0.99	1.98

the plate outside the wave boundary layer. The amplitude of the pressure correction is 45–50% of the total recorded force, i.e., the pressure force is about equal to the shear force.

The LUCIO data include two sequences of random waves in still water and with an orthogonal current superimposed. The MAST3 data include one sequence of random waves in still water and with two near-orthogonal currents superimposed; one opposing and one following. The data used here are the friction coefficients calculated from the half-cycle amplitude of the shear stress τ_m (between consecutive maxima and minima) and the corresponding amplitude of wave-induced velocity. Statistical analysis of the data has been performed in order to make a proper comparison with the theoretical approach.

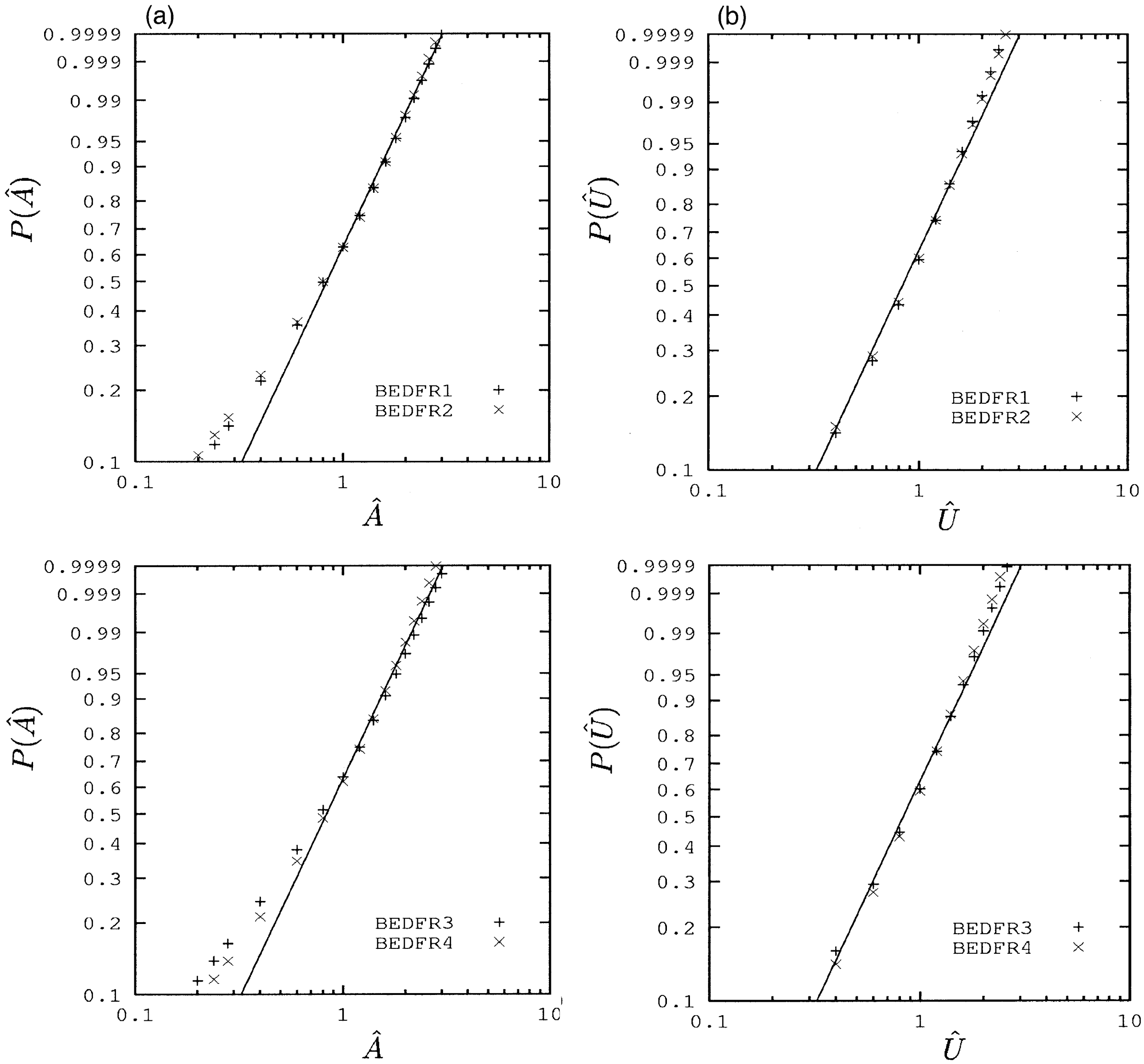

Fig. 1. Probability distribution of normalized bed orbital displacement amplitude ($\hat{A}$) and velocity amplitude ($\hat{U}$) in Weibull scale: — Rayleigh distribution, Eq. (5) with (a) $\hat{x} = A/A_{rms}$, (b) $\hat{x} = U/U_{rms}$; other symbols represent LUCIO data. See also Table 1.

The actual test conditions for the LUCIO and MAST3 data sets are given in Table 1, together with some analysis results which will be discussed subsequently. Here $T_z = 2\pi/\omega_z = 2\pi A_{rms}/U_{rms}$ is the mean zero-crossing wave period, and $\bar{U}$ is the depth-averaged current velocity over the water depth $h = 0.50$ and 0.49 m for LUCIO and MAST3, respectively. The roughness Reynolds number is defined as $Re = k_N u^*/\nu$, where ν is the kinematic viscosity of the fluid, and $u^* = (\tau_m/\rho)^{1/2}$ is the friction velocity. The LUCIO and MAST3 data represent rough turbulent flow (i.e., $Re > 70$, see, e.g., Schlichting, 1979), but appear to be in the lower A/z_0 range, i.e., $1 \lesssim A/z_0 \lesssim 300$ (see Fig. 3) and $3 \lesssim A/z_0 \lesssim 60$ (see Fig. 4), respectively. Overall, it appears that the Soulsby friction coefficient formula in Eqs. (2) and (3) underpredicts the data. Therefore, the M95 approach is modified to cover the rough turbulent flow regime for the lower A/z_0 range for random waves alone as well as random waves plus current by utilizing the observed properties of the LUCIO and MAST3 data sets.

A consequence of the narrow-band assumption is that A and U both are Rayleigh-distributed (see Eq. (5)), and thus it is of interest to compare the directly measured data of A and U (i.e., determined from half-cycle analysis of individual random waves) with the narrow-band assumption upon which the approach is based. Fig. 1a and b shows $P(\hat{A})$ and $P(\hat{U})$, respectively, for the LUCIO data in Weibull scale together with the Rayleigh distribution. Here $\hat{A} = A/A_{rms}$ and $\hat{U} = U/U_{rms}$. In Weibull scale, the ordinate and abscissa are taken as $\ln[-\ln(1 - P(\hat{x}))]$ and $\ln \hat{x}$, respectively. Fig. 2a and b shows similar results for the MAST3 data. For the LUCIO data there appear to be differences between the Rayleigh distribution and the data for $P(\hat{A})$ for lower values of $\hat{A}$ (Fig. 1a). There also appear to be significant differences between the Rayleigh distribution and the data for $P(\hat{A})$ and $P(\hat{U})$ for the MAST3 following current condition (Fig. 2). However, overall it appears that the Rayleigh distribution can be taken to represent the data for the larger values of $\hat{A}$ and $\hat{U}$ for waves alone as well as waves plus current except for the MAST3 t3030FC record.

Figs. 3 and 4 show the results of fitting Eq. (2) to the half-cycle data for the LUCIO and MAST3 data set records, respectively. The values of c and d are given in Table 1. One should note that the best fit to all the LUCIO half-cycle data gives $c = 17.3$ and $d = 0.998$, while the corresponding values for the MAST3 half-cycle data are $c = 13.1$ and $d = 0.95$. Thus, it appears that the d value is close to 1.0. For $d = 1$, the special case of the Weibull shape parameter $\beta = 2$ in Eq. (6) coincides with the Rayleigh

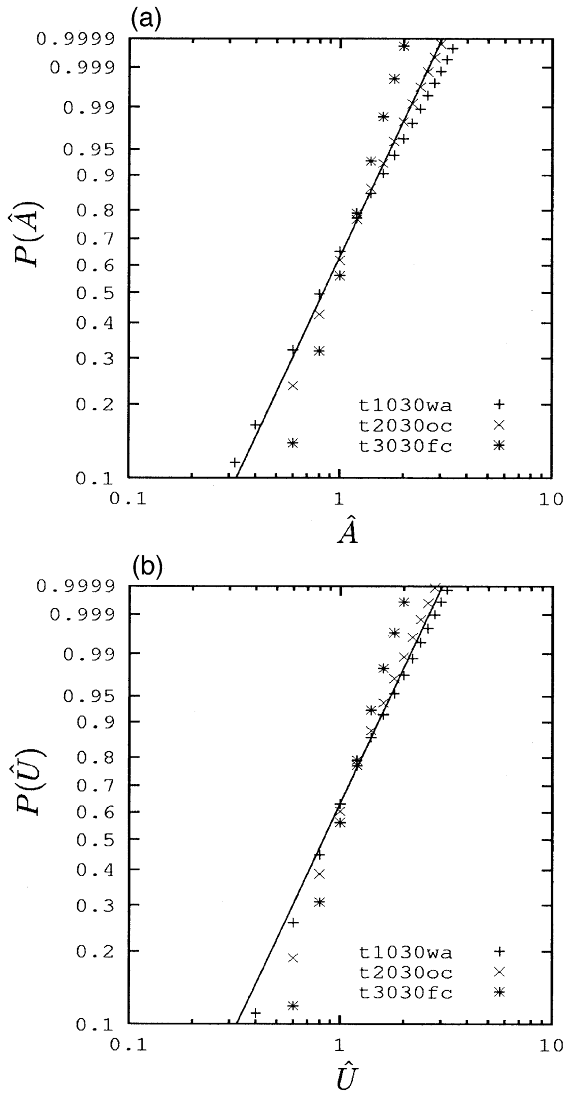

Fig. 2. Probability distribution of normalized bed orbital displacement amplitude ($\hat{A}$) and velocity amplitude ($\hat{U}$) in Weibull scale: — Rayleigh distribution, Eq. (5) with (a) $\hat{x} = A/A_{rms}$, (b) $\hat{x} = U/U_{rms}$; other symbols represent MAST3 data. See also Table 1.

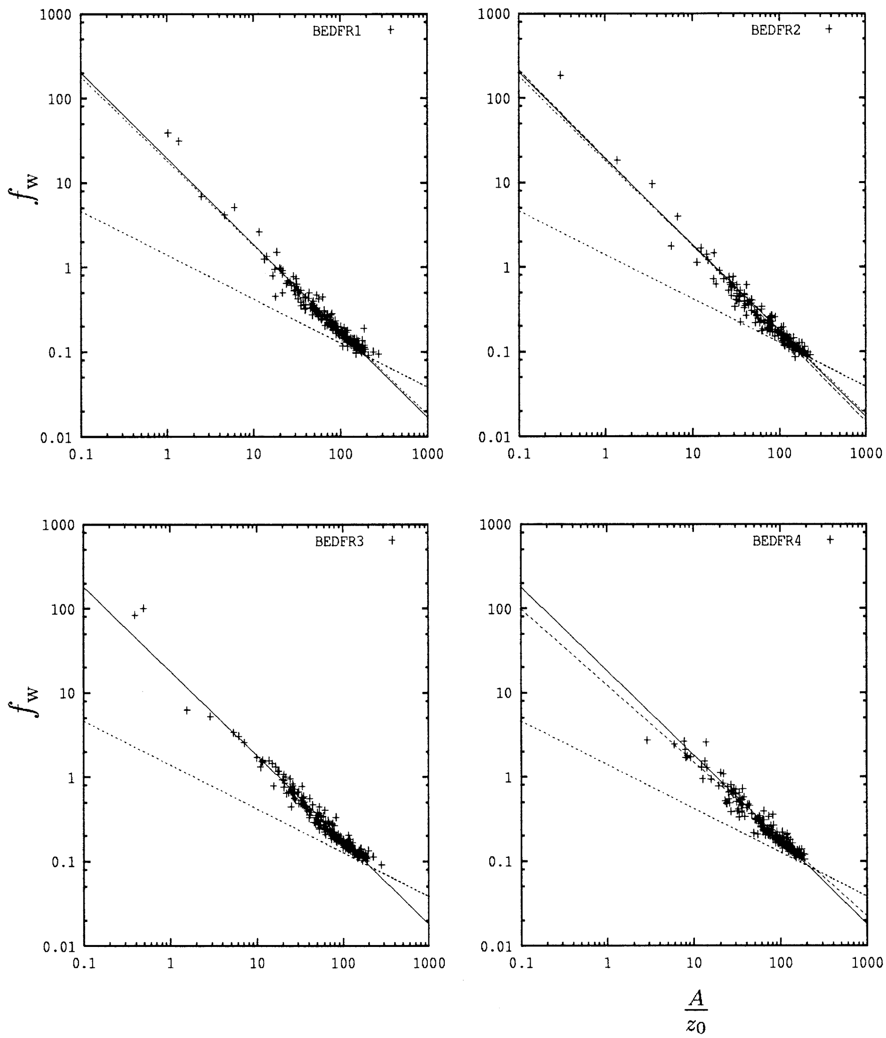

Fig. 3. Friction coefficient versus amplitude to roughness ratio for the LUCIO half-cycle data: — best fit of Eq. (2) to BEDFR1 data; - - - best fit of Eq. (2) to BEDFR2 data; — best fit of Eq. (2) to BEDFR3; - - - best fit of Eq. (2) to BEDFR4 data; · · · Soulsby et al. (1993); · · · · · · Eq. (9); other symbols represent LUCIO data. See also Table 1.

distribution, i.e., suggesting that t can be represented by the Rayleigh distribution. Considering the range of c values obtained as the best fit to the LUCIO and MAST3 half-cycle data and the d values which are close to 1 for all the records, a reasonable compromise between simplicity and accuracy can be accomplished by taking $d = 1.0$ and $c = 18.0$ (which are the values for the LUCIO BEDFR3 record). Thus, the wave friction coefficient in Eq. (2) covering the A/z_0-range of the LUCIO and MAST3 data yields

$$f_w = 18\left(\frac{A}{z_0}\right)^{-1} \text{for } 1 \lesssim \frac{A}{z_0} \lesssim 300. \tag{9}$$

As shown in Figs. 3 and 4, Eq. (9) represents the half-cycle data quite well in this range considering the scatter in the data. The Soulsby formula is also

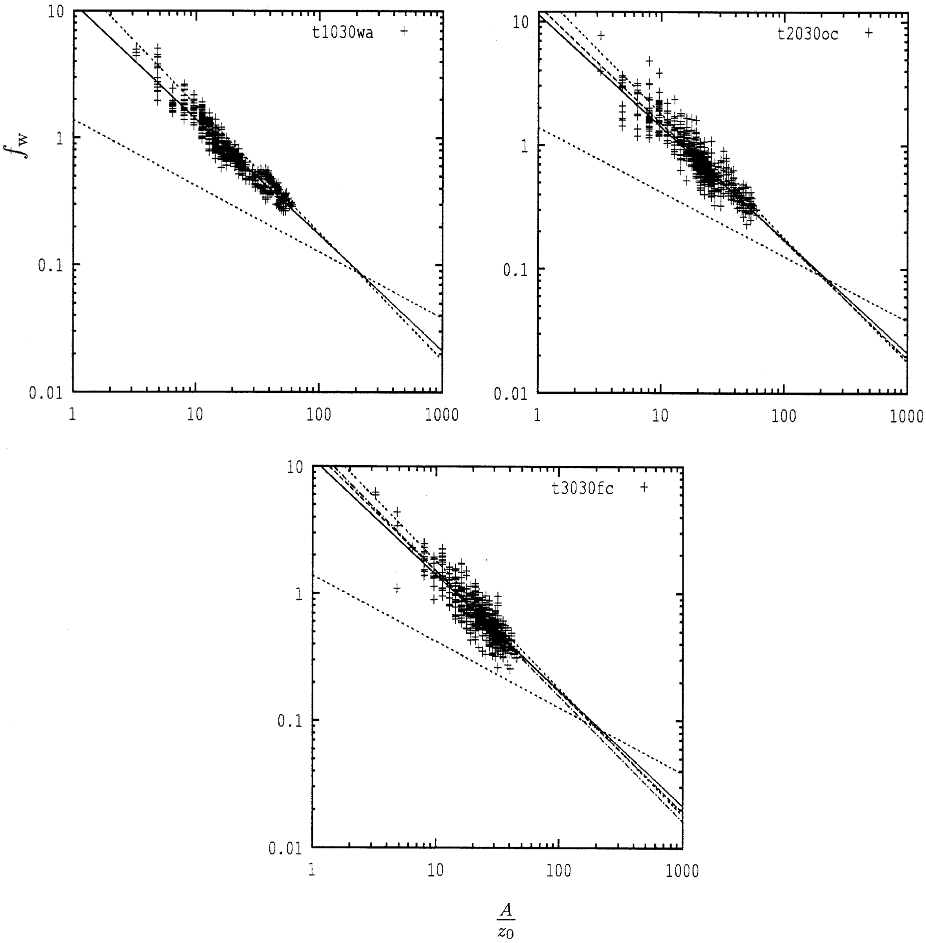

Fig. 4. Friction coefficient versus amplitude to roughness ratio for the MAST3 half-cycle data: — best fit of Eq. (2) to t1030WA data; - - - best fit of Eq. (2) to t2030OC data; -· -· best fit of Eq. (2) to t3030FC data. ··· Soulsby (1997); ··· ··· Eq. (9); other symbols represent MAST3 data. See also Table 1.

included for comparison. Furthermore, the f_w-data are not altered by adding a current, as should be expected for orthogonal as well as near-orthogonal currents superimposed on waves for lower A/z_0 values, as long as the current is not too dominant (see Soulsby et al., 1993; Simons et al., 1994, 2000).

However, so far the magnitudes of the bed shear stress maxima have been considered. It should be noted that even for a weak current having a direction relative to harmonic waves, the instantaneous bed shear stress changes direction (see Fig. 5), and consequently, the direction of the maximum shear stress in combined wave–current motion τ_{wcmax} is turned away from the wave direction ϕ. An estimate of the current effect on the relative direction between τ_m and τ_{wcmax} can be obtained by utilizing the results in Soulsby (1997, Chap. 5.3). The current friction factor C_D is defined as $\tau_c = \rho C_D \overline{U}^2$ where τ_c is the shear stress due to current alone, and C_D is a function of the roughness to water depth ratio z_0/h. The wave friction factor is defined in Eq. (1). Now an "order of magnitude" calculation can be made by using Soulsby (1997, Eq. (69)) for the mean bed shear stress, i.e.,

$$\tau_{mean} = \tau_c \left[1 + 1.2 \left(\frac{\tau_m}{\tau_c + \tau_m} \right)^{3.2} \right]. \tag{10}$$

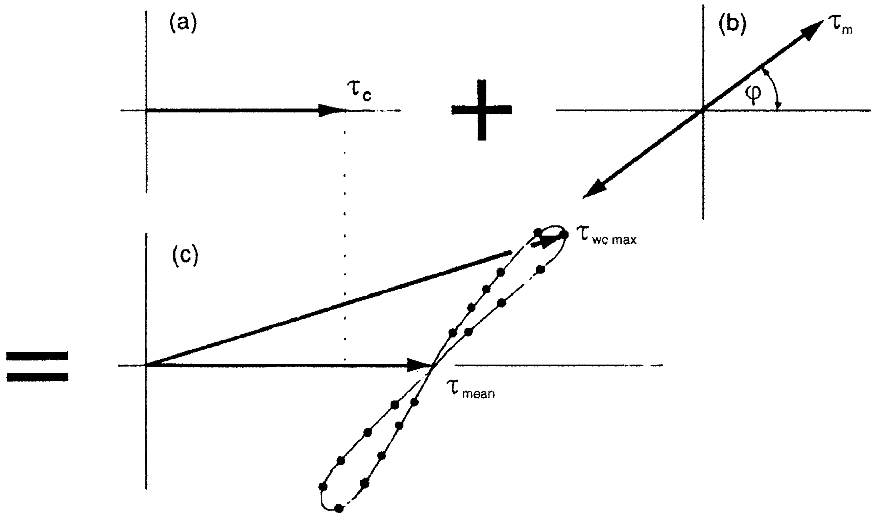

Fig. 5. Schematic of instantaneous bed shear stresses for wave-current interaction: (a) the current alone stress (τ_c), and (b) the wave alone stress amplitude $= \tau_m$, combine nonlinearly to give (c) the locus of the combined stresses having τ_{wcmax} (reproduced from Soulsby et al., 1993).

Furthermore, assume that the wave to current velocity ratio $U/\overline{U} \gtrsim 1$ and $C_D/f_w \lesssim 0.1$, giving $\tau_c \lesssim 0.1\tau_m$, which is the case for wide ranges of z_0/h and A/z_0; see the forthcoming discussion related to the results given in Table 3. Then it follows from Eq. (10) that $\tau_{mean} \approx 2\tau_c$, showing the nonlinear enhancement of the mean bed shear stress due to the presence of waves. For orthogonal waves and current, which represent the largest difference in direction, vectorial addition of $\vec{\tau}_{mean}$ and $\vec{\tau}_m$ gives an estimate of $\vec{\tau}_{wcmax}$. This gives that $\vec{\tau}_{wcmax}$ is turned about 10° away from $\vec{\tau}_m$. This suggests that for the wave–current interaction considered here, the difference in direction between τ_m and τ_{wcmax} is insignificant. Thus, τ_m is a good approximation to τ_{wcmax}, and accordingly Eq. (9) gives a good estimate of the friction factor for wave–current interaction in the given A/z_0 range for practical purposes. Further discussion on the ranges of z_0/h and A/z_0 in which the present approach is valid will be given in the forthcoming.

It should be noted that an alternative to Eq. (10) would be to use the results of You (1995), who derived a simple formula to calculate τ_{mean} in a combined wave–current flow. He concluded that the increase of bed shear stress in the presence of waves was linearly proportional to the wave velocity U and independent of the relative bed roughness A/z_0 and the relative angle between waves and current. It appears that an "order of magnitude" calculation using $\tau_c \approx 0.1\tau_m$ in You (1995, Eq. (7)) gives $\tau_{mean} \approx 2\tau_c$, which agrees with the results using Eq. (10) in the range of validity of Eq. (9), i.e., $1 \lesssim A/z_0 \lesssim 300$.

One should note that Simons et al. (1996) concluded that the Swart (1974) f_w formula gave excellent agreement with the measured wave friction factors for regular as well as irregular waves. However, the purpose here is not necessarily to replace Swart's formula, but to present a simple f_w formula, which can be inverted and thereby used to make transformation of random variables to obtain an analytical distribution of the shear stress maxima. This is not possible by using, e.g., the Swart formula. However, if the Swart formula is used in Eq. (4), it is expected that the probability distribution of the shear stress maxima will be very close to a Weibull distribution. This is supported by Holmedal et al. (2000, Fig. 3), which used Monte-Carlo simulations on a f_w formula that is very close to Swart's.

2.3. Modified M95 approach predictions *vs.* measurements

Figs. 6 and 7 show the probability distribution function of the normalized bottom shear stress t in Weibull scale for the LUCIO and MAST3 data set

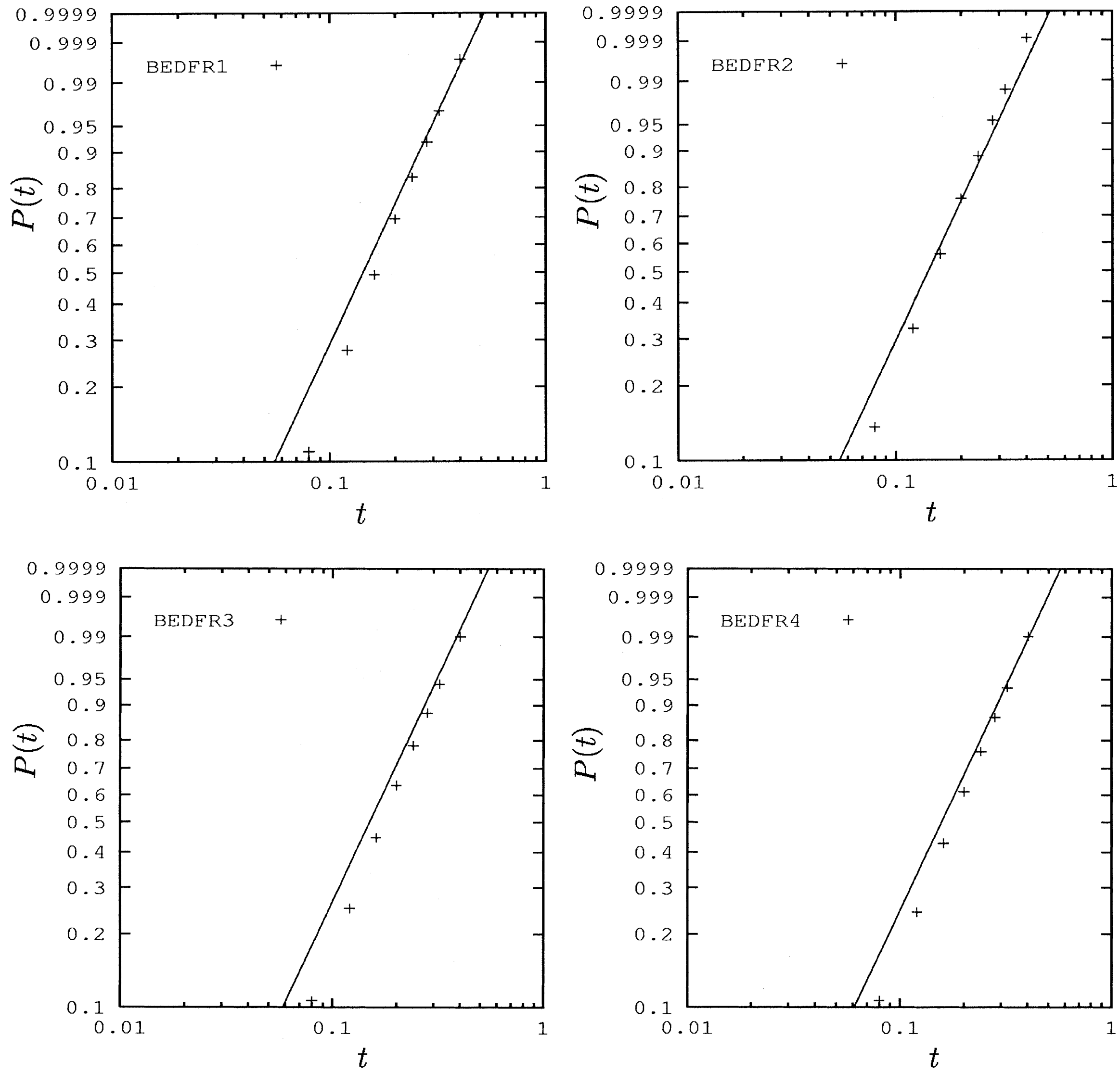

Fig. 6. Probability distribution function of normalized maximum bottom shear stress in Weibull scale: — Eq. (11) ; + LUCIO data. See also Table 1.

records, respectively. One should note that the model here is the Rayleigh distribution given by Eqs. (6)–(8) with $c = 18$, $d = 1$, and $\beta = 2$, i.e.,

$$P(t) = 1 - \exp\left[-\left(\frac{t}{\alpha}\right)^2\right];$$

$$\alpha = 18\left(\frac{A_{\mathrm{rms}}}{z_0}\right)^{-1}, t \geq 0. \tag{11}$$

It appears that Eq. (11) gives a good representation of the LUCIO data for larger values of t (Fig. 6). This is also the case for the MAST3 t1030WA record (Fig. 7). However, differences between the model and the data are observed for the two other MAST3 records; particularly for record t3030FC representing the following current condition (Fig. 7). In these cases, the model gives a smaller probability than the data for larger values of t. For the t3030FC

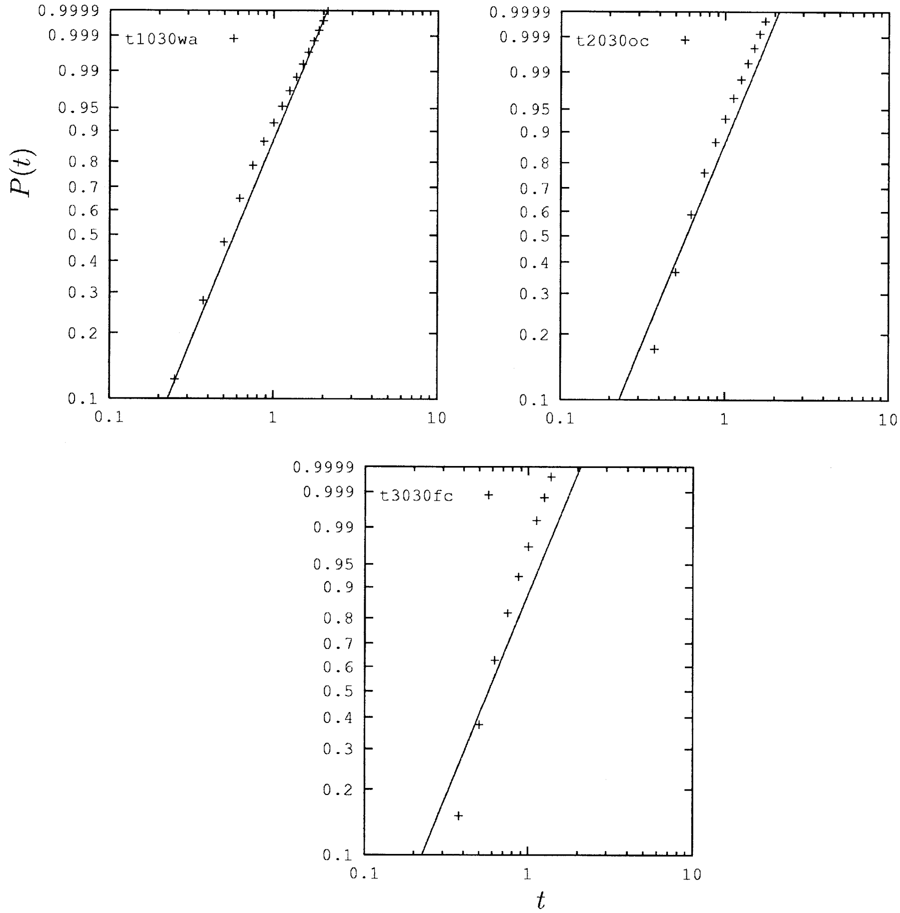

Fig. 7. Probability distribution function of normalized maximum bottom shear stress in Weibull scale: — Eq. (11); + MAST3 data. See also Table 1.

record, these differences are most likely attributed to the poor agreement between the Rayleigh distribution and the data for $P(\hat{A})$ and $P(\hat{U})$ which were noted in Fig. 2.

Fig. 8 shows the measured versus the predicted values of $E[t]$, σ_t, t_{rms} as well as $t_{1/n}$ and $E[t_{1/n}]$ for $n=3$ and $n=10$ for the LUCIO and MAST3 data set records. The predicted to measured ratio ranges of these characteristic statistical values are given in Table 2. The predictions are given by Eqs. (A6)–(A10), respectively, for the Rayleigh distribution in Eq. (11). Overall it appears that these characteristic statistical values are well predicted for the LUCIO data, while they are slightly overpredicted for the MAST3 data. Note that those MAST3 data values, which are most overpredicted represent record t3030FC, for which $\hat{A}$ and $\hat{U}$ were not well represented by the Rayleigh distribution.

Fig. 9 shows the measured versus the predicted values of $E[t_N]$ and t_N (which are defined in Appendix A) for the LUCIO data set records. $E[t_N]$ and t_N are both estimates of the largest value in a time series containing N values of individual shear stress maxima. A measured value corresponding to these estimates is obtained by selecting the largest value of t in the time series. The predicted to measured ratio ranges of these values are given in Table 2. The predictions are given by Eqs. (A11) and (A12), respectively, for the Rayleigh distribution in Eq. (11). It appears that $E[t_N]$ and t_N are overpredicted

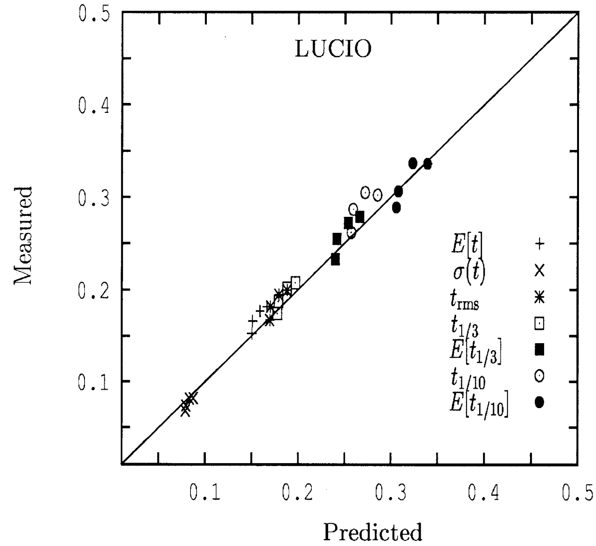

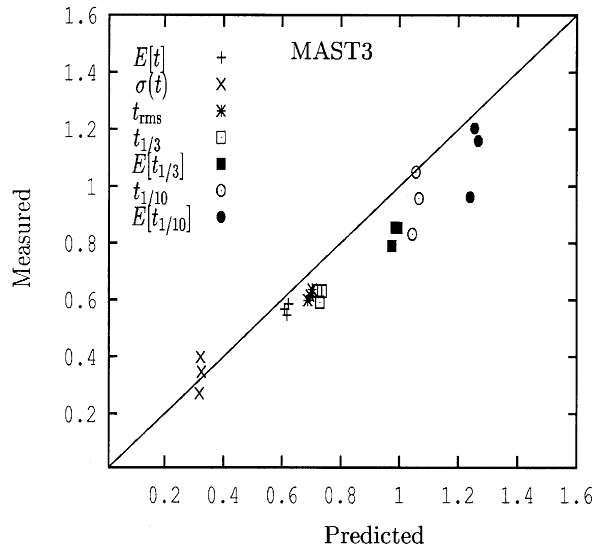

Fig. 8. Measured versus predicted values of σ_t, $E[t]$, t_{rms}, $t_{1/n}$ and $E[t_{1/n}]$ for $n = 3$, 10.

except for one data set, which is slightly underpredicted. The MAST3 data are not included here because limitations within the wave generation software used as input to the wave generator in the wave tank, resulted in the irregular time series for obliquely incident waves containing repeating sequences of relatively short duration. Overall, the results given in Figs. 8 and 9 and Table 2 show that the predictions

Table 2
Predicted to measured ratio ranges for the characteristic statistical values

Data set	σ_t	$E[t]$	t_{rms}	$t_{1/3}$	$E[t_{1/3}]$	$t_{1/10}$	$E[t_{1/10}]$	t_N	$E[t_N]$
LUCIO	1.02–1.15	0.90–0.98	0.92–1.01	0.93–1.02	0.93–1.03	0.89–0.98	0.96–1.01	0.91–1.16	0.96–1.22
MAST3	0.81–1.17	1.08–1.13	1.11–1.15	1.14–1.25	1.15–1.23	1.01–1.25	1.04–1.29	–	–

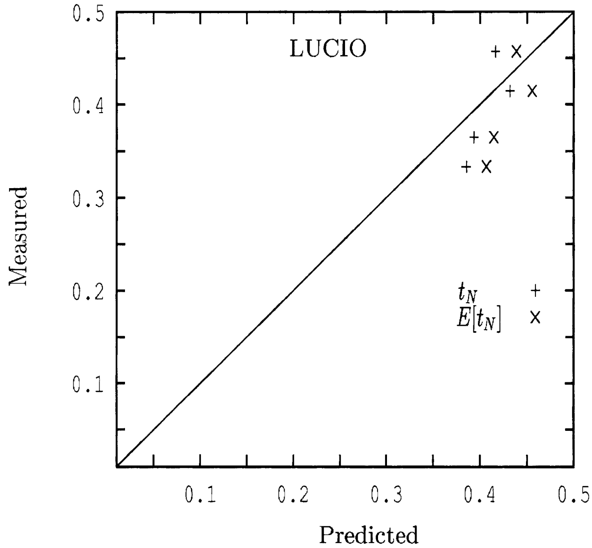

Fig. 9. Measured versus predicted values of the largest normalized maximum bottom shear stress for the LUCIO data.

deviate less than 20% from most of the measurements.

2.4. Friction coefficient: regular versus irregular waves

Some further aspects of the LUCIO and MAST3 data sets are shown in Fig. 10. Fig. 10 shows the friction coefficients based on characteristic statistical values versus the corresponding characteristic statistical orbital displacement amplitude to roughness ratios. The friction coefficients considered here are

$$f_{\mathrm{w,rms}} = \frac{(\tau_{\mathrm{m}}/\rho)_{\mathrm{rms}}}{\frac{1}{2}U_{\mathrm{rms}}^2}; \tag{12}$$

$$f_{\mathrm{w},1/n} = \frac{(\tau_{\mathrm{m}}/\rho)_{1/n}}{\frac{1}{2}U_{1/n}^2}, \qquad n = 3,10; \tag{13}$$

$$\bar{f}_{\mathrm{w},1/n} = \frac{E[(\tau_{\mathrm{m}}/\rho)_{1/n}]}{\frac{1}{2}\left(E[U_{1/n}]\right)^2}, \qquad n = 3,10; \tag{14}$$

$$f_{\mathrm{w,max}} = \frac{(\tau_{\mathrm{m}}/\rho)_{\mathrm{max}}}{\frac{1}{2}U_{\mathrm{max}}^2}. \tag{15}$$

Here, the subscript “max” corresponds to the largest value in a time series. It should be noted that the values shown in Fig. 10 are those calculated from the half-cycle data. In the upper part of Fig. 10, the various friction coefficient data are identified together with Eq. (9). However, in the lower part of the figure, the same data are replotted, identified as separate data sets only, and compared with regular wave data as well as friction coefficient formulas for regular waves.

There appears to be an agreement between some of the irregular wave data and the regular wave data in the same amplitude to roughness ratio regime as well as with some of the friction coefficient formulas for regular waves. The LUCIO data representing $f_{\mathrm{w,rms}}$, $f_{\mathrm{w},1/3}$ and $\bar{f}_{\mathrm{w},1/3}$ agree well with predictions by the Kamphuis (1975) formula for regular waves, while the other LUCIO data tend to be underpredicted. The MAST3 data representing $f_{\mathrm{w,rms}}$ and $f_{\mathrm{w},1/3}$ agree well with predictions by the Jonsson and Carlsen (1976) formula for regular waves, while the other MAST3 data are underpredicted. One should note that the Swart formula is very close to that of Jonsson and Carlsen (1976). Furthermore, the LUCIO and MAST3 data sets appear to be in agreement with some of the regular wave data of Kamphuis (1975) and Sleath (1987) in the same A/z_0 range. It appears that Eq. (9) lies within 25% of the LUCIO

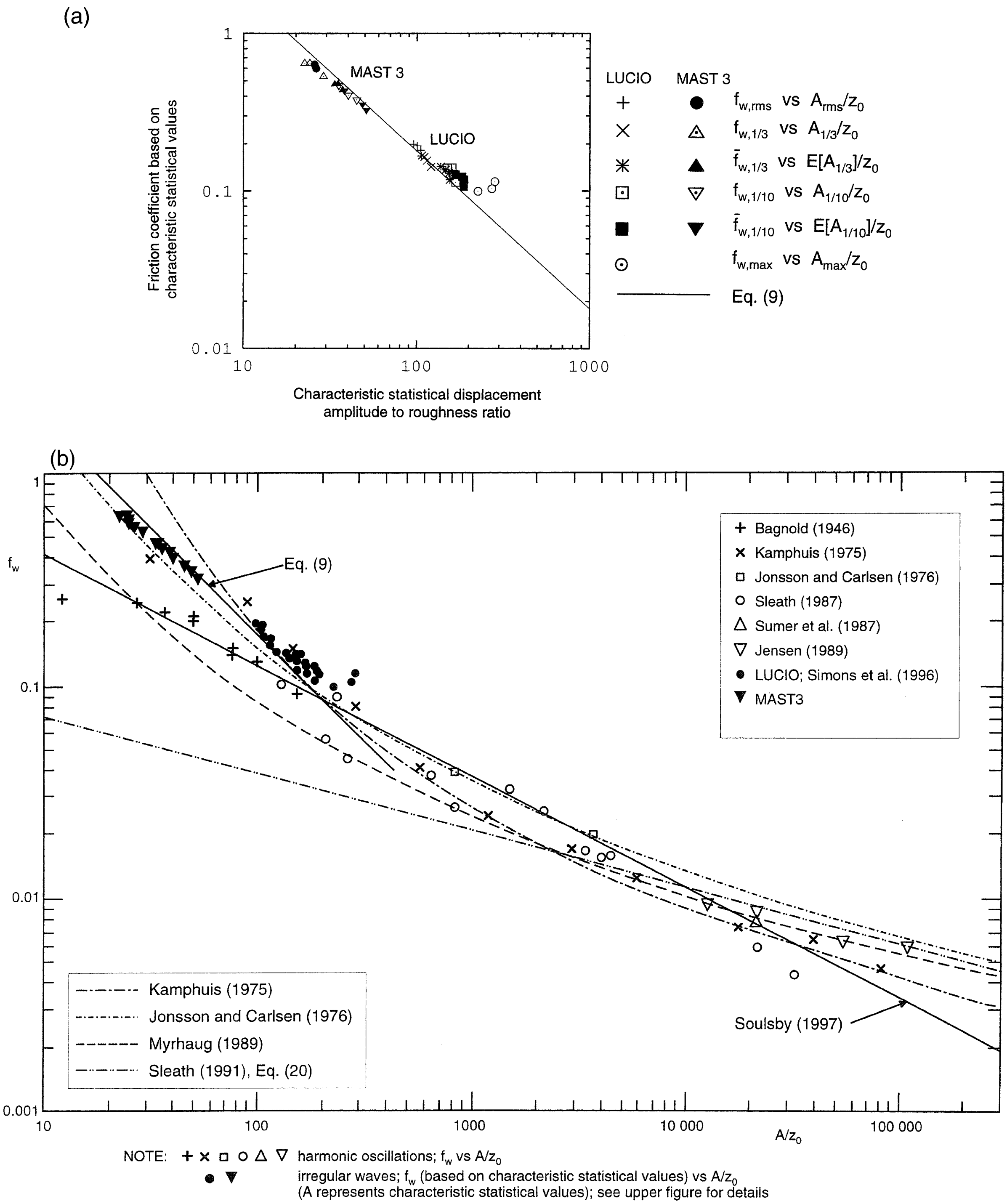

NOTE: + × □ ○ △ ▽ harmonic oscillations; f_w vs A/z_0

● ▼ irregular waves; f_w (based on characteristic statistical values) vs A/z_0

(A represents characteristic statistical values); see upper figure for details

Fig. 10. Friction coefficient versus amplitude to roughness ratio (Jensen, 1989; Myrhaug, 1989; Sumer et al., 1987).

and MAST3 data, except for two of the LUCIO data points for $f_{\mathrm{w,max}}$ versus $A_{\max}/z_0$. Eq. (9) also lies within 40% of the Kamphuis (1975) and two of the Sleath (1987) data for $A/z_0 < 300$. As noted earlier, the irregular wave data are not altered significantly by adding a current.

Sleath (1991) has given a friction coefficient formula for sinusoidal waves which takes into account the total horizontal force acting on the bed, i.e., consisting of the shear stress on the bed plus the components due to the mean pressure gradient acting on the exposed surface of the bed roughness. The latter component was calculated for grains of sediment tightly packed in a single layer on a flat plate. Sleath examined data in the range $1 \leq A/k_N \leq 120$ (i.e., $30 \leq A/z_0 \leq 3600$) and obtained

$$f_{\mathrm{w}} = (B^2 + C^2 + 2BC\sin\theta)^{1/2}, \tag{16}$$

where $\theta = 22.5°$, and

$$B = 0.048\left(\frac{A}{k_N}\right)^{-0.25}, \tag{17}$$

$$C = 0.60\left(\frac{A}{k_N}\right)^{-1}. \tag{18}$$

Here, B and C represent the components due to the shear stress and the mean pressure gradient, respectively. For large and small values of A/k_N, the terms B and C, respectively, dominate in Eq. (16). Thus, by using $z_0 = k_N/30$, good approximations for Eq. (16) are given by

$$f_{\mathrm{w}} = 18\left(\frac{A}{z_0}\right)^{-1} \tag{19}$$

for lower values of A/z_0, and

$$f_{\mathrm{w}} = 0.112\left(\frac{A}{z_0}\right)^{-0.25} \tag{20}$$

for higher values of A/z_0. Eq. (19) appears to coincide with Eq. (9). However, it is important to note that there is an inconsistency between the physical conditions of the LUCIO and MAST3 data and conditions that Eq. (19) represents. That is, Eq. (19) represents pressure gradient effects, whereas the data represent just the shear stress component (the total force having been corrected for pressure gradient effects).

The shear stress part of the Sleath formula given by Eq. (20), which is shown in Fig. 10, significantly underpredicts the LUCIO and MAST3 data as well as the other data in the lower A/z_0 range. Sleath himself pointed out the anomalies associated with Eq. (20) without offering any definite explanation for the disagreement between the curve representing Eq. (20) and the experimental results for which f_{w} should be independent of the pressure gradient term, as shown in Sleath (1991, Fig. 8). Sleath also observed "that experimental determination of f_{w} in oscillatory flow is subject to significant errors". However, concerning the LUCIO and MAST3 data there is no reason to believe either that the data are not correctly measured or that they are inadequately corrected for the pressure contribution. As mentioned earlier, the pressure force is about equal to the shear force, and therefore the agreement with Sleath's pressure term actually confirms the validity of the present test results as well as the correction procedure. However, it does not help explaining why the Sleath shear prediction does not work. One should also note that the drag is dominated by viscous effects in the lower A/z_0 range of the LUCIO and MAST3 data, which affects the near-bed velocity profile and thereby the bed shear stress. When viscous effects are important, the shear stress is not scaled with A/z_0 alone, i.e., the bed roughness geometry may have significant influence on the near-bed flow, which until now has not been properly accounted for. Therefore, generally there is large uncertainty associated with the bed shear stress for $A/z_0 \lesssim 900$. Thus, no firm explanation for the disagreement between Eq. (20) and the LUCIO and MAST3 data can presently be given.

One should note that the friction coefficients defined in Eqs. (13)–(15) reduce to Eq. (2) for any c and d values by replacing f_{w} and A with the appropriate friction coefficient and the corresponding statistical quantity of A, respectively. Thus it appears that Eq. (2) with $c = 18$ and $d = 1$, corresponding to Eq. (9), lies within 25% of most of the data, which is considered to be an adequate representation of the friction coefficients for irregular waves alone as well as irregular waves plus current in the amplitude to roughness ratio range considered, regardless of which of the friction coefficients in Eqs. (13)–(15) are used. Furthermore, by combining Eqs. (12), (4) and (A8) it follows that the rms friction coefficient is given as

$$f_{w,rms} = \Gamma\left(1+\frac{2}{\beta}\right)c\left(\frac{A_{rms}}{z_0}\right)^{-d}. \quad (21)$$

For $d=1$ and $\beta=2$, $\Gamma(1+2/\beta)=1$; otherwise, $\Gamma(1+2/\beta)\neq 1$. Thus, concerning the rms friction coefficient, Eq. (2) can only be used by replacing f_w and A with $f_{w,rms}$ and A_{rms}, respectively, for $d=1$. For other d-values, Eq. (2) has to be multiplied by the factor $\Gamma(1+2/\beta)$ if f_w and A are replaced by $f_{w,rms}$ and A_{rms}, respectively.

2.5. Extension of the M95 approach

Based on the previous discussions and the observations from Fig. 10, it is suggested to take the distribution function of the bottom shear stress maxima for random waves plus current as given in Eqs. (6)–(8) together with: Eq. (9) for lower A/z_0 values; Eqs. (2) and (3) for intermediate A/z_0 values; and Eq. (20) for larger A/z_0 values. More specifically, this means that Eqs. (6)–(8) should be used with

$$c = 18,\ d = 1.0 \text{ for } 20 \lesssim A/z_0 \lesssim 200, \quad (22)$$

$$c = 1.39,\ d = 0.52 \text{ for } 200 \lesssim A/z_0 \lesssim 11000, \quad (23)$$

$$c = 0.112,\ d = 0.25 \text{ for } 11000 \lesssim A/z_0. \quad (24)$$

As previously noted, the Swart formula is very close to that of Jonsson and Carlsen, and as observed in Fig. 10 both are as good as the formulas described by Eqs. (22)–(24). However, the latter formulas make it possible to derive Eq. (6) analytically.

This approach is taken to be valid for random waves plus current as long as the effect of the current is not stronger than the effect of the waves. It is possible to be more specific about the range of validity of this approach by making the following "order of magnitude" considerations. The observations by comparing the current friction factor C_D in Soulsby (1997, Fig. 10) with the wave friction factor f_w shown in Fig. 10 are summarized in Table 3. From Table 3, it appears that f_w is at least a factor of 10 larger than C_D in the given ranges of z_0/h and A/z_0 when the classes above the diagonal in Table 3 are excluded. By considering the wave to current velocity ratio $U/\bar{U} \gtrsim 1$, it follows that the wave shear stress to current shear stress ratio $\tau_m/\tau_c \gtrsim 10$ for these parameter ranges. By utilizing this in Soulsby's parameterization of, e.g., Fredsøe's (1984) model for bed shear stresses under regular waves plus current (Soulsby, 1997, Chap. 5.3), it follows that the maximum shear stress in the wave–current motion is dominated by the wave shear stress τ_m for any angle between waves and current. One should note that the parameterization of the Fredsøe model represents the actual model quite well (Soulsby et al., 1993), and overall it is representative of the main features of the bed shear stresses for regular waves plus current (Soulsby, 1997, Chap. 5.3). Thus the proposed model in Eqs. (6)–(8) together with Eqs. (22)–(24) represents an extension of the M95 approach. It should be noted, however, that the present approach should be compared with irregular wave data for $A/z_0 \gtrsim 200$. Otherwise, the present results suggest that this approach can be used as first approximation to represent the bottom friction under random waves plus current when there is weak wave–current interaction effect on the maximum bottom shear stresses. This occurs for $U/\bar{U} \gtrsim 1$ and for the ranges of A/z_0 and z_0/h below the diagonal of Table 3.

One should note that it might happen that the random events t occur in more than one of the A/z_0 ranges given in Eqs. (22)–(24). However, since the A/z_0 range given by Eq. (23) is quite wide, t will most likely not cover more than two different A/z_0

Table 3
Typical values of C_D and f_w in the given ranges of z_0/h and A/z_0

$z_0/h \lesssim$	$A/z_0 \lesssim$		
	2×10^2	2×10^3	2×10^4
10^{-2}	$C_D \lesssim 0.01$	$C_D \lesssim 0.01$	$C_D \lesssim 0.01$
	$f_w \gtrsim 0.1$	$f_w \gtrsim 0.03$	$f_w \gtrsim 0.01$
10^{-4}	$C_D \lesssim 0.003$	$C_D \lesssim 0.003$	$C_D \lesssim 0.003$
	$f_w \gtrsim 0.1$	$f_w \gtrsim 0.03$	$f_w \gtrsim 0.01$
10^{-6}	$C_D \lesssim 0.001$	$C_D \lesssim 0.001$	$C_D \lesssim 0.001$
	$f_w \gtrsim 0.1$	$f_w \gtrsim 0.03$	$f_w \gtrsim 0.01$

ranges, i.e., those covered by Eqs. (22) and (23), or Eqs. (23) and (24). In such a case, it is recommended to use the rms value (i.e., A_{rms}/z_0) to determine which A/z_0 range to use, since this is the value commonly used to represent an equivalent sinusoidal wave.

3. Conclusions

The bottom friction in random waves plus current flow is presented. The model extends the Myrhaug (1995) approach for random waves alone to cover random waves plus current for weak wave–current interaction effect on the individual maximum bed shear stresses, as long as the wave to current velocity ratio exceeds one over wide ranges of A/z_0 and z_0/h of practical importance. The current effect on the direction of the maximum bed shear stress is estimated to be less than 10° within the range of validity of the approach. Overall, the present approach gives an adequate representation of the Simons et al. (1996) and MAST3 data, which cover the lower orbital displacement amplitude to roughness ratio regime. It appears that:

(1) The probability distribution function of seabed shear stress maxima is well represented by the Rayleigh distribution for larger shear stress values for most of the data. The best agreement is found between the model and the Simons et al. (1996) data. The difference between the model and the MAST3 record representing the following current condition is significant. This disagreement is attributed to the poor agreement between the data and the Rayleigh distribution of the bed orbital displacement amplitude and velocity amplitude. In this case, the model gives a smaller probability than the data for larger shear stress values.

(2) The predictions of the characteristic statistical values of the normalized seabed shear stress maxima $E[t]$, σ_t, t_{rms}, $t_{1/3}$, $t_{1/10}$, $E[t_{1/3}]$, $E[t_{1/10}]$, $E[t_N]$ and t_N lie within 20% of most of the measurements.

(3) The friction coefficients based on characteristic statistical values versus the corresponding characteristic statistical orbital displacement amplitude to roughness ratios show good agreement with regular wave data in the same amplitude to roughness range. Some of the irregular wave friction coefficients also agree well with the standard formulas of Swart (1974), Kamphuis (1975) and Jonsson and Carlsen (1976) for fully rough turbulent flow for regular waves.

A formula based on the Rayleigh distribution of shear stress maxima lies within 25% of most of the irregular wave friction factor data. This suggests that Eq. (9) gives a reasonably good representation for irregular waves in the amplitude to roughness ratio range 20–200, regardless of which of the friction coefficients in Eqs. (12)–(15) are used.

Acknowledgements

This work was undertaken as part of the MAST3 project “The Kinematics and Dynamics of Wave–Current Interactions”. It was funded by the Commission of the European Union Directorate General for Science, Research and Development under Contract No. MAS3-CT95-0011.

Appendix A. The M95 shear stress distribution under random waves

In M95, the distribution function of the bottom shear stress maxima was determined by assuming that: (1) the free surface elevation ζ is a stationary Gaussian narrow-band random process with zero expectation described by the single-sided spectral density $S_{\zeta\zeta}(\omega)$ with the angular wave frequency ω, and (2) the friction coefficient for sinusoidal waves are valid for random waves as well. The second assumption implies that each wave is treated individually, and consequently that the friction coefficient is taken to be constant for a given wave situation. The accuracy of this assumption should be validated by using a full boundary layer model to calculate the shear stress under random waves. However, results from some preliminary studies were discussed in M95 and Myrhaug and Hansen (1997), and overall the results suggest that the M95 approach is adequate as a first approximation and can be used to predict, e.g., integrated effects such as bedload sediment transport with a reasonable degree of accuracy.

Based on the present assumptions, the (instantaneous) time-dependent bed orbital displacement and velocity a and u, respectively, are both stationary

Gaussian narrow-band processes with zero expectations and with single-sided spectral densities

$$S_{aa}(\omega) = \frac{S_{\zeta\zeta}(\omega)}{\sinh^2 kh}, \tag{A1}$$

$$S_{uu}(\omega) = \omega^2 S_{aa}(\omega) = \frac{\omega^2 S_{\zeta\zeta}(\omega)}{\sinh^2 kh}. \tag{A2}$$

Here, k is the wave number determined from the dispersion relationship $\omega^2 = gk \tanh kh$ for linear waves, h is the water depth, and g is the acceleration of gravity.

Now the orbital displacement amplitude at the seabed (A) and the orbital velocity amplitude at the seabed (U) are both Rayleigh-distributed with the probability distribution functions given by Eq. (5) with $\hat{A} = A/A_{\text{rms}}$ and $\hat{U} = U/U_{\text{rms}}$, respectively. Here the rms (root-mean-square) values A_{rms} and U_{rms} are related to the zeroth moments m_{0aa} and m_{0uu} of the amplitude and velocity spectral densities, respectively, (corresponding to the variances of the amplitude (σ_{aa}^2) and the velocity (σ_{uu}^2)), given by

$$A_{\text{rms}}^2 = 2m_{0aa} = 2\sigma_{aa}^2 = 2\int_0^\infty S_{aa}(\omega)\,\mathrm{d}\omega, \tag{A3}$$

$$U_{\text{rms}}^2 = 2m_{0uu} = 2\sigma_{uu}^2 = 2\int_0^\infty S_{uu}(\omega)\,\mathrm{d}\omega. \tag{A4}$$

From Eqs. (A4) and (A2), it also appears that $m_{0uu} = m_{2aa}$, where m_{2aa} is the second moment of the amplitude spectral density. Thus the mean zero-crossing wave frequency ω_z is obtained from the spectral moments of a as

$$\omega_z = \left(\frac{m_{2aa}}{m_{0aa}}\right)^{1/2} = \left(\frac{m_{0uu}}{m_{0aa}}\right)^{1/2} = \frac{U_{\text{rms}}}{A_{\text{rms}}} \tag{A5}$$

where Eqs. (A3) and (A4) have been used. It should be noted that the result Eq. (A5) is valid for a stationary Gaussian stochastic process.

Now Eqs. (6)–(8) are obtained by using Eqs. (1) and (2) with $A = U/\omega$ and ω replaced by ω_z from Eq. (A5); then it follows that τ_m is distributed as U^{2-d}, from which Eqs. (6)–(8) follow by transformation of random variables by using Eq. (5) with $\hat{x} = U/U_{\text{rms}}$. This model using c and d in Eq. (3) has only been compared with estimates of seabed shear stresses under random waves from field measurements. In that case, good agreement was found between predictions and data from the Strait of Juan de Fuca, Washington State (Myrhaug et al., 1998).

From the probability distribution characteristic statistical values of the bottom shear stress maxima are obtained.

The expected value of t, $E[t]$, and the standard deviation of t, σ_t, given by, respectively (see, e.g., Bury, 1975)

$$E[t] = \alpha\Gamma\left(1 + \frac{1}{\beta}\right), \tag{A6}$$

$$\sigma_t = \alpha\left[\Gamma\left(1 + \frac{2}{\beta}\right) - \Gamma^2\left(1 + \frac{1}{\beta}\right)\right]^{1/2}, \tag{A7}$$

where Γ is the gamma function.

The rms-value of t is given as

$$t_{\text{rms}} \equiv \left(E[t^2]\right)^{1/2} = \alpha\left[\Gamma\left(1 + \frac{2}{\beta}\right)\right]^{1/2}. \tag{A8}$$

The value of t which is exceeded by the probability $1/n$, $t_{1/n}$, and the expected value of the $1/n$ largest values of t, $E[t_{1/n}]$ are given by

$$t_{1/n} = \alpha(\ln n)^{1/\beta}, \tag{A9}$$

$$E[t_{1/n}] = n\alpha\Gamma\left(1 + \frac{1}{\beta}, \ln n\right), \tag{A10}$$

where $\Gamma(\cdot,\cdot)$ is the incomplete gamma function.

The expected largest value among N values is given by (see, e.g., Bury, 1975)

$$E[t_N] = \alpha(\ln N)^{1/\beta}\left(1 + \frac{0.5772}{\beta\ln N}\right). \tag{A11}$$

The first term in Eq. (A11) can be interpreted as the "characteristic largest value", t_N, which has, on the average, only one exceedance in a sample of size N, i.e., $1 - P(t_N) = 1/N$, giving

$$t_N = \alpha(\ln N)^{1/\beta}. \tag{A12}$$

References

Bagnold, R.A., 1946. Motion of waves in shallow water. Interaction between waves and sand bottom. Proc. R. Soc., Ser. A 187, 1–15.

Bury, K.V., 1975. Statistical Models in Applied Science. Wiley, New York.

Fredsøe, J., 1984. Turbulent boundary layer in wave–current motion. J. Hydraul. Eng. ASCE 110, 1103–1120.

Grass, A.J., Simons, R.R., MacIver, R.D., Mansour-Tehrani, M., Kalopedis, A., 1995. Shear cell for direct measurement of fluctuating bed shear stress vector in combined wave/current flow, Proc. XXVIth IAHR Congress: Hydraulic Research and its Applications next Century–HYDRA 2000, London, UK, Paper 1C8, pp. 415–420.

Holmedal, L.E., Myrhaug, D., Rue, H., 2000. Seabed shear stresses under irregular waves plus current from Monte Carlo simulations of parameterized models. Coastal Eng. 39, 123–147.

Jensen, B.L., 1989. Experimental Investigation of Turbulent Oscillatory Boundary Layers, Series Paper 45, Inst. Hydrodyn. and Hydr. Eng., Tech. Univ. Denmark, Lyngby.

Jensen, B.L., Sumer, B.M., Fredsøe, J., 1989. Turbulent oscillatory boundary layers at high Reynolds numbers. J. Fluid Mech. 206, 266–297.

Jonsson, I.G., Carlsen, N.A., 1976. Experimental and theoretical investigations in an oscillatory turbulent boundary layer. J. Hydraul. Res. 14, 45–60.

Kamphuis, J.W., 1975. Friction factors under oscillatory waves. ASCE J. Waterw., Harbors, Coastal Eng. Div. 10 (WW2), 135–144.

Lambrakos, K.F., 1982. Seabed wave boundary layer measurements and analysis. J. Geophys. Res. 87 (C6), 4171–4189.

Madsen, O.S., 1994. Spectral wave–current bottom boundary layer flows. Proc. 24th Conf. Coastal Eng., ASCE, Kobe, Japan, vol. 1, pp. 384–398.

Myrhaug, D., 1989. A rational approach to wave friction coefficients for rough, smooth and transitional turbulent flow. Coastal Eng. 13, 11–21.

Myrhaug, D., 1995. Bottom friction beneath random waves. Coastal Eng. 24, 259–273.

Myrhaug, D., Hansen, E.H., 1997. Long-term distribution of seabed shear stresses beneath random waves. Coastal Eng. 31, 327–337.

Myrhaug, D., Lambrakos, K.F., Slaattelid, O.H., 1992. Wave boundary layer in flow measurements near the seabed. Coastal Eng. 18, 153–181.

Myrhaug, D., Slaattelid, O.H., Lambrakos, K.F., 1998. Seabed shear stresses under random waves: predictions versus estimates from field measurements. Ocean Eng. 25, 907–916.

Nielsen, P., 1992. Coastal Bottom Boundary Layers and Sediment Transport. World Scientific Publishing, Singapore.

Ockenden, M.C., Soulsby, R.L., 1994. Sediment transport by currents plus irregular waves. Report SR 376, HR Wallingford, Wallingford, UK.

Schlichting, H., 1979. Boundary-Layer Theory. 7th edn. McGraw-Hill, New York.

Simons, R.R., Kyriacou, A., Soulsby, R.L., Davies, A.G., 1988. Predicting the nearbed turbulent flow in waves and currents. Proc. IAHR Symposium on Mathematical Modelling of Sediment Transport in The Coastal Zone, Copenhagen, Denmark, pp. 33–47.

Simons, R.R., Grass, T.J., Saleh, W.M., Tehrani, M.M., 1994. Bottom shear stresses under random waves with a current superimposed. Proc. 24th Conf. Coastal Eng., ASCE, Kobe, Japan, vol. 1, pp. 565–578.

Simons, R.R., MacIver, R.D., Saleh, W.M., 1996. Kinematics and shear stresses from combined waves and longshore currents in the UK Coastal Research Facility. Proc. 25th Conf. Coastal Eng., ASCE, Orlando, pp. 3481–3494.

Simons, R.R., Myrhaug, D., Thais, L., Chapalain, G., Holmedal, L.E., MacIver, R., 2000. Bed friction in combined wave–current flows. Proc. 27th Conf. Coastal Eng., ASCE, Sydney, Australia.

Sleath, J.F.A., 1987. Turbulent oscillatory flow over rough beds. J. Fluid Mech. 182, 369–409.

Sleath, J.F.A., 1991. Velocities and shear stresses in wave–current flows. J. Geophys. Res. 96 (C8), 15237–15244.

Sleath, J.F.A., 1995. Coastal bottom boundary layers. Appl. Mech. Rev., ASME 48 (9), 589–599.

Soulsby, R.L., 1997. Dynamics of Marine Sands. A Manual for Practical Applications. Thomas Telford, London, UK.

Soulsby, R.L., Hamm, L., Klopman, G., Myrhaug, D., Simons, R.R., Thomas, G.P., 1993. Wave–current interaction within and outside the bottom boundary layer. Coastal Eng. 21, 41–69.

Sumer, B.M., Jensen, B.L., Fredsøe, J., 1987. Turbulence in oscillatory boundary layers. In: Comte-Bellot, C., Mathieu, E. (Eds.), Advances in Turbulence. Springer, Berlin, pp. 556–567.

Swart, D.H., 1974. Offshore sediment transport and equilibrium beach profiles. Delft Hydraulics Lab. Publ. 131, Delft, The Netherlands.

Trowbridge, J.H., Agrawal, Y.C., 1995. Glimpses of a wave boundary layer. J. Geophys. Res. 100 (C10), 20729–20743.

You, Z.J., 1995. Increase of current bottom shear stress due to waves. Coastal Eng. 26, 291–295.

Zhao, Y., Anastasiou, K., 1993. Bottom friction effects in the combined flow field of random waves and currents. Coastal Eng. 19 (3,4), 223–243.